Available online at www.sciencedirect.com
ScienceDirect
Tectonophysics 453 (2008) 276–294
TECTONOPHYSICS
www.elsevier.com/locate/tecto

Geometry of the fault zone of the 2003 Ms=7.5 Chuya earthquake and associated stress fields, Gorny Altai

Oxana V. Lunina [a,*], Andrei S. Gladkov [a], Igor S. Novikov [b], Anna R. Agatova [b], Evgenii M. Vysotskii [b], Alexei A. Emanov [c]

[a] Institute of the Earth's Crust SB RAS, Lermontov Street 128, Irkutsk, 664033, Russia
[b] Institute of Geology SB RAS, Academician Koptyug Pr. 3, Novosibirsk, 630090, Russia
[c] Geophysical Survey SB RAS, Academician Koptyug Pr. 3, Novosibirsk, 630090, Russia

Received 9 January 2006; accepted 4 October 2007
Available online 6 February 2008

Abstract

The co-seismic deformations produced during the September 27, 2003 Chuya earthquake (Ms=7.5) that affected the Gorny Altai, Russia, are described and discussed along a 30 km long segment. The co-seismic deformations have manifested themselves both in unconsolidated sediments as *R*- and *R′*-shears, extension fractures and contraction structures, and in bedrock as the reactivation of preexisting schistosity zones and individual fractures, as well as development of new ruptures and coarse crushing zones. It has been established that the pattern of earthquake ruptures represents a typical fault zone trending NW–SE with a width reaching 4–5 km and a dextral strike–slip kinematics. The initial stress field that produced the whole structural pattern of co-seismic deformations during the Chuya earthquake, is associated with a transcurrent regime with a NNW–SSE, almost N–S, trending of compressional stress axis (σ_1), and a ENE–WSW, almost E–W, trending of tensional stress axis (σ_3). The state of stress in the newly-formed fault zone is relatively uniform. The local stress variations are expressed in insignificant deviation of σ_1 from N–S to NW–SE or NE–SW, in short-term fluctuations of relative stress values in keeping their spatial orientations, or in a local increase of the plunge angle of the σ_1. The geometry of the fault zone associated with the Chuya earthquake has been compared with the mechanical model of fracturing in large continental fault zones with dextral strike–slip kinematics. It is apparent that the observed fracture pattern corresponds to the late disjunctive stage of faulting when the master fault is not fully developed but its segments are already clearly defined. It has been shown that fracturing in widely different rocks follows the common laws of the deformation of solid bodies, even close to the Earth surface, and with high rates of movements.

Keywords: Chuya earthquake; Fault zone; Co-seismic deformations; Stress fields; Gorny Altai

1. Introduction

The Ms=7.5 Chuya earthquake of September 27, 2003, is the strongest event in the southeastern part of the Gorny Altai (Western Siberia, Russia) over the instrumental period of seismological observations (Fig. 1). In contrast to the Mongolian and Gobi Altai catastrophic earthquakes (Trifonov and Makarov, 1988; Baljinnyam et al., 1993; Leontyev and Rogozhin, 1995; Cunningham et al., 1996; 1997), only two strong earthquakes with M≥6 were recorded in the broader Gorny Altai region before the Chuya earthquake (Novikov, 2004). These are the earthquake of September 21, 1923 (M=6) and the Zaisan earthquake of June 14, 1990 (M=6.6). The former earthquake was not field-checked, and its precise location is unknown. The hypocenter of the Zaisan earthquake was at a depth of 35–40 km that suggested the relatively modest "linear morphogenic effects" (according to Caputo, 2005a) at the surface. The recorded ruptures were apparently due to secondary causes, seismovibrational or seismogravitational (Leontyev and Rogozhin, 1995) and could be considered as "areal seismogenetic features" (Caputo, 2005a). Compared to these previous earthquakes, the Chuya earthquake is unique for several reasons. Firstly, its epicenter is located in the center of

* Corresponding author. Fax: +7 3952 426900.
E-mail address: lounina@crust.irk.ru (O.V. Lunina).

0040-1951/$ - see front matter © 2008 Elsevier B.V. All rights reserved.
doi:10.1016/j.tecto.2007.10.010

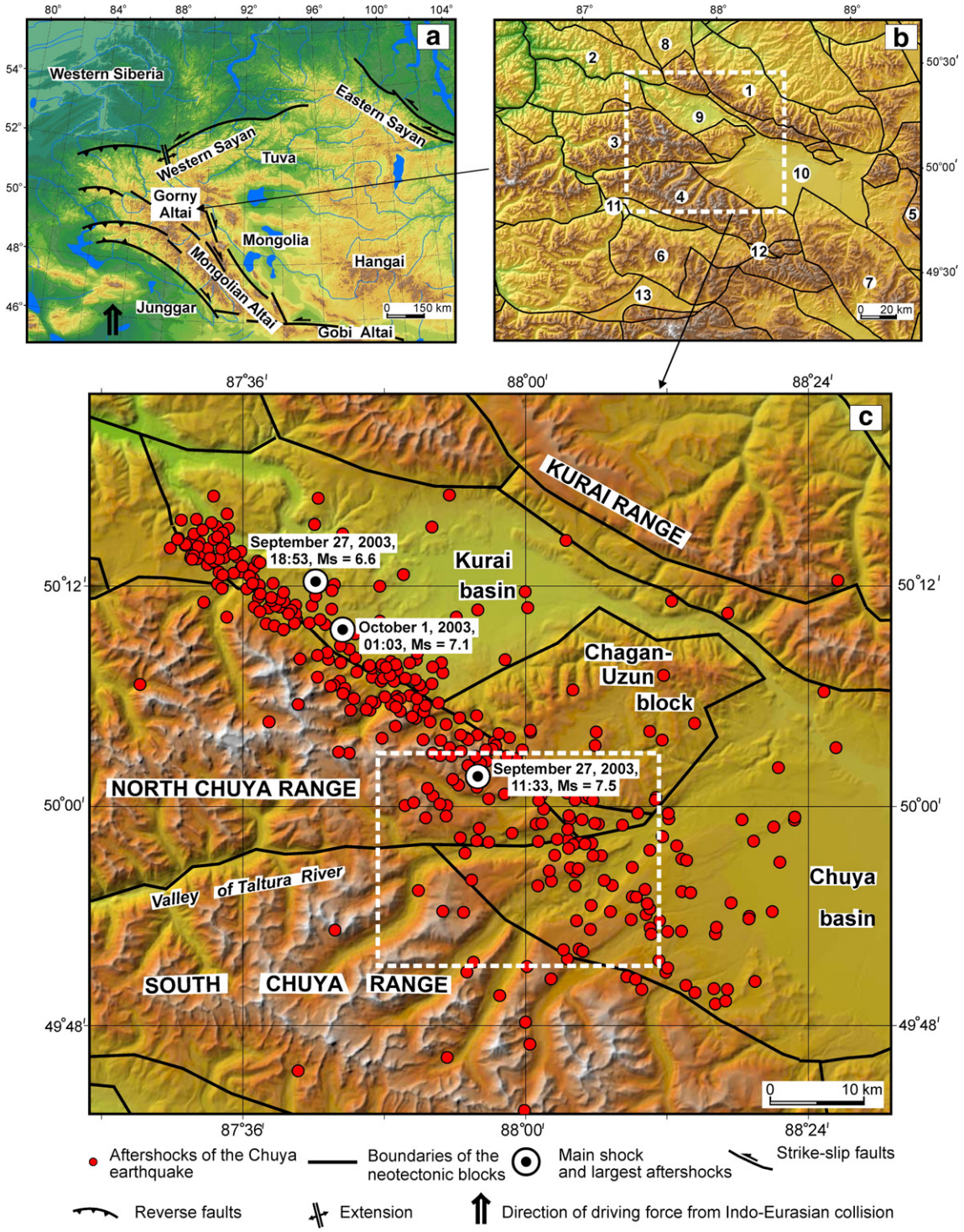

Fig. 1. Framework of the research area: (a) regional topography, geodynamics (after Novikov, 2004) and location of the Gorny Altai; (b) the main morphostructural elements of the Southeastern Altai: ranges: Kurai (1), Aigulak (2), North Chuya (3), South Chuya (4) and Chikhachev (5); plateauxes: Ukok (6) and Sailyugem (7); inter-mountainous basins: Sorulukol (8), Kurai (9), Chuya (10), Samakhin (11), Tarkhatin(12) and Bertek (13); (c) the strongest seismic events in September–October, 2003 and epicenters of aftershocks. The map of the main morphostructural elements of the Southeastern Altai was compiled by Novikov I.S. The data on the aftershock locations have been obtained by Geophysical Survey of the Siberian Branch of Russian Academy of sciences (SB RAS). Magnitudes of the main shock and two strongest aftershocks are presented from the Harvard SMT Catalog of earthquakes (http://www.seismology.harvard.edu). Dotted line in Fig. 1b indicates Fig. 1c. Dotted line in Fig. 1c shows the investigated area represented in Fig. 2.

the local network of ten digital seismic stations (Altai seismological test area) installed by the Geophysical Survey SB RAS in August 2002, therefore allowing specific observations of the seismic process in the epicentral area before and after the earthquake (Goldin et al., 2004). Abundance of qualitative data and applying of new approach gave a quite

accurate determination of hypocenter of the main shock at a depth of 8.76 km (Emanov and Leskova, 2005). Secondly, the co–seismic deformations resulting from the earthquake were systematically observed. Thirdly, a sizeable segment of the newly-formed pattern of the surface ruptures turned out to be accessible for detailed field investigation (Geodakov et al., 2003; Vysotskii et al., 2004; Lunina et al., 2005a, 2006).

The first results of the preliminary field investigations in the epicentral area of the Chuya earthquake were published by Geodakov et al. (2003). They traced a 20 km long pattern of surface ruptures trending WNW–ESE. Our research carried out in May 2004, shows that the surface ruptures extend for more than 30 km (Lunina et al., 2005a; 2006). In July 2004, two of the authors (E.M. Vysotskii and I.S. Novikov) enlarged the study area and reported that the zone of the co-seismic deformations exceeds 56 km. They collected additional data on rupture tracks with using handheld GPS navigators, allowing essentially to specify the geometry of the newly-formed rupture zone and therefore to compile a new map of its inner structure in comparison with that published in the previous paper (Lunina et al., 2006). In the present paper, for the first time, we also show a detailed view of several fault segments produced during the Chuya earthquake and infer the stress trajectories in the investigated area.

Thus, the aim of this work is to improve the previous results based on new data and to supplement the traditional seismo-geological observations by tectonophysical analysis that allows (1) the comparison of the surface ruptures to deformation models of solid bodies, (2) to compare the existing fault pattern with the newly-formed one, and (3) to reconstruct the stress field associated with the 2003 seismic events. These objectives will better constrain the regional tectonics of the Gorny Altai as well as improve the understanding of developing fault zones.

2. Tectonic setting

The Altai mountainous system is located in the region of Russia, Kazakhstan, Mongolia and China and forms a part of the Central-Asian mobile belt. The mountain structures of the Russian sector of the Altai (Gorny Altai) are the northern continuation of the Mongolian and Gobi Altai structures and western branch of the Altai-Sayan fold system (Rogozhin et al., 1998; Rogozhin and Platonova, 2002; Geodakov et al., 2003; Novikov, 2004) (Fig. 1a). The southeastern part of the Gorny Altai (Southeastern Altai) contains a number of ranges (Kurai, Aigulak, North Chuya, South Chuya and Chikhachev) and Ukok and Sailyugem plateaus separated by river valleys and inter-mountainous basins (Sorulukol, Kurai, Chuya, Samakhin, Tarkhatin and Bertek) (Fig. 1b). Most of the area is located at elevations higher than 2000 m. Axial parts of the ranges often exceed 3500 m.

A model of the Cenozoic orogeny and formation of tectonic structure of the Altai has been recently proposed in the light of the concept of plate tectonics (Novikov, 2004). According to the model, the Altai is a mobile zone of first order in the Cenozoic structure of Central Asia (Fig. 1a). It separates the Junggar and Tuva-Mongolian micro-plates and is bordered by the West-Siberian plate on the north. The Altai orogeny has a transpressive character (term "transpressive" is used according to Sanderson and Marchini, 1984) and is due to the convergence of these micro-plates. The Junggar and Tuva-Mongolian micro-plates converge with the dextral strike–slip, and all the major

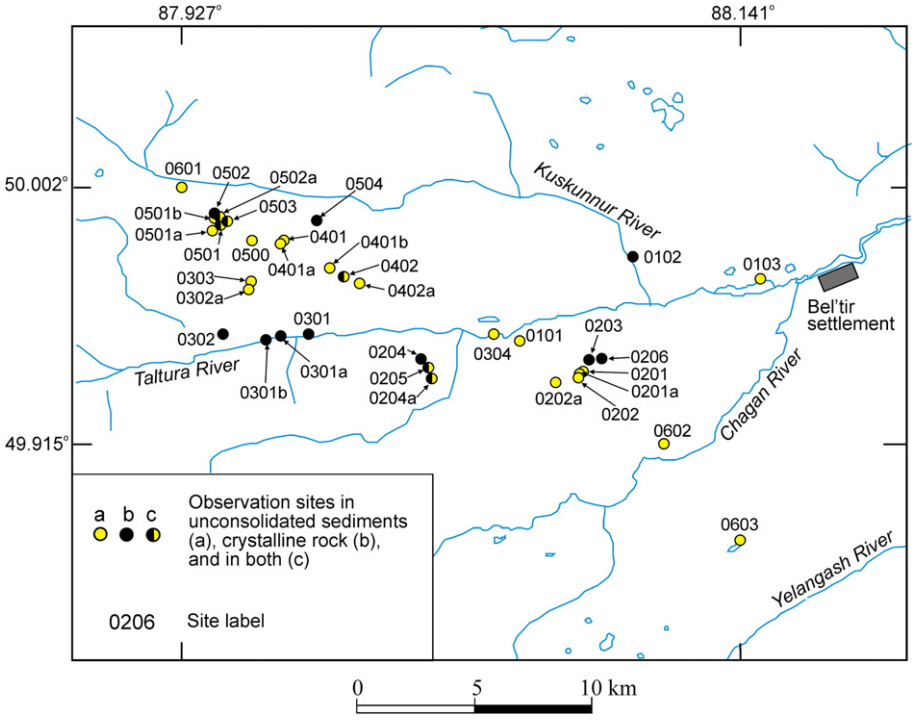

Fig. 2. Location of the observation sites.

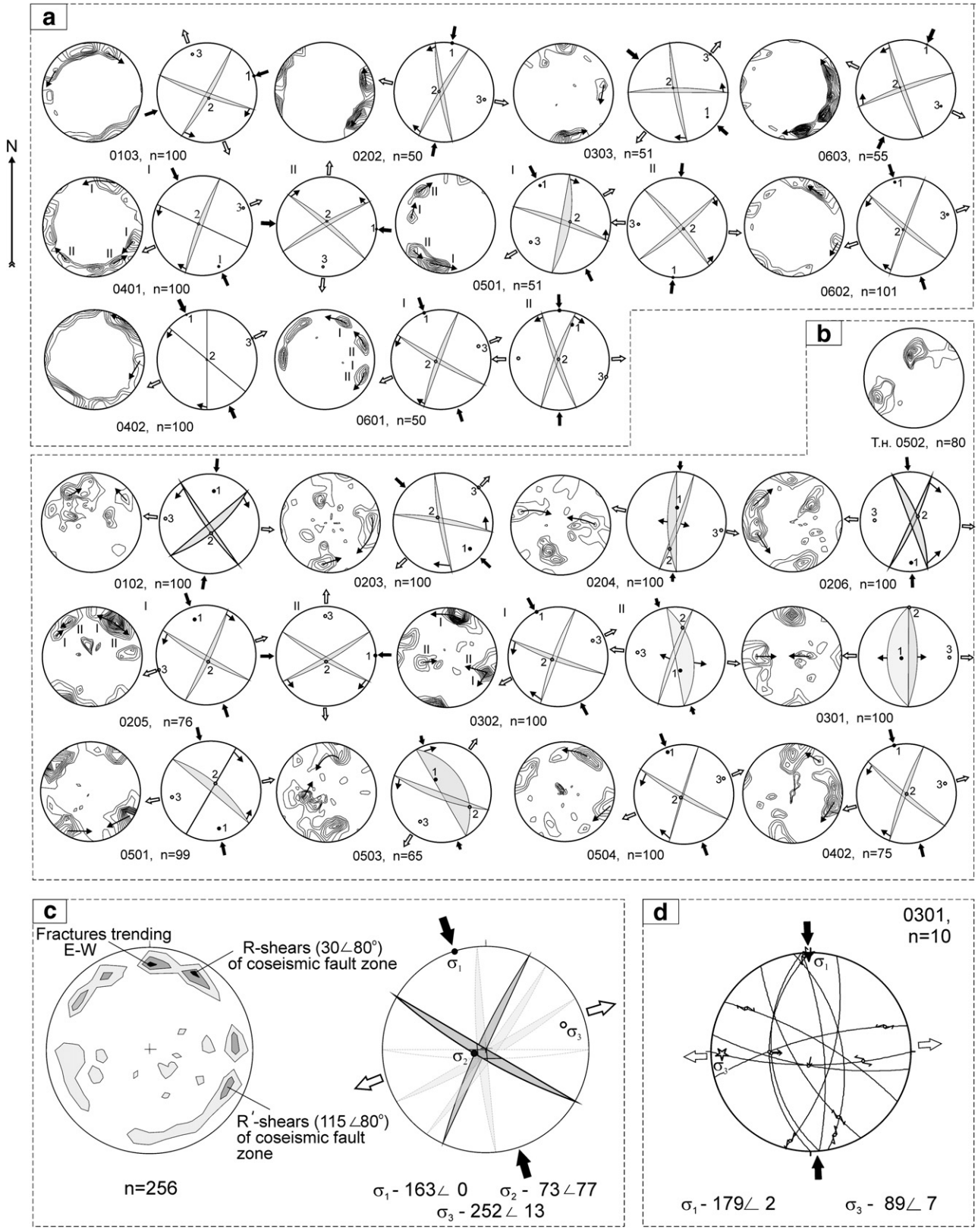

Fig. 3. Fracture diagrams and reconstructions of the principal stress directions (equal-area upper hemisphere projection): (a) fractures measured in Pleistocene–Holocene unconsolidated sediments (intensity isolines are 3.5, 4.5, 5.5% and >5.5%); (b) fractures measured in pre-Cenozoic bedrock (intensity isolines are 1.5, 2.5, 3.5, 4.5% and >4.5%). Arrows inside the diagrams in figures (a) and (b) show the scattering directions within maxima, thus indicating the conjugate systems by Nikolaev's method (1992). In the cases of two sets of conjugate shear fracture systems, they are marked by Roman numerals. 0601 — site label, n — number of measurements. 1, 2 and 3 are the compressional (σ_1), intermediate (σ_2) and tensional (σ_3) stress axes, respectively; (c) synoptic diagram of fracturing maxima from figures (a) and (b) and stress field solution from *R*- and *R*′-shears (intensity isolines are 1.5, 2.5, 3.5%); (d) principal stress axes obtained with the multiple inverse method (Yamaji, 2000) at site 0301.

fault systems, the direction of which coincides generally with the NW–SE trend of the mobile zone, also have the strike–slip kinematics (Novikov, 2004). Most of the main structures have a reverse component of displacement that causes high-altitude differentiation of blocks and formation of mountainous relief. The local extension zones edge the strike–slip faults. The

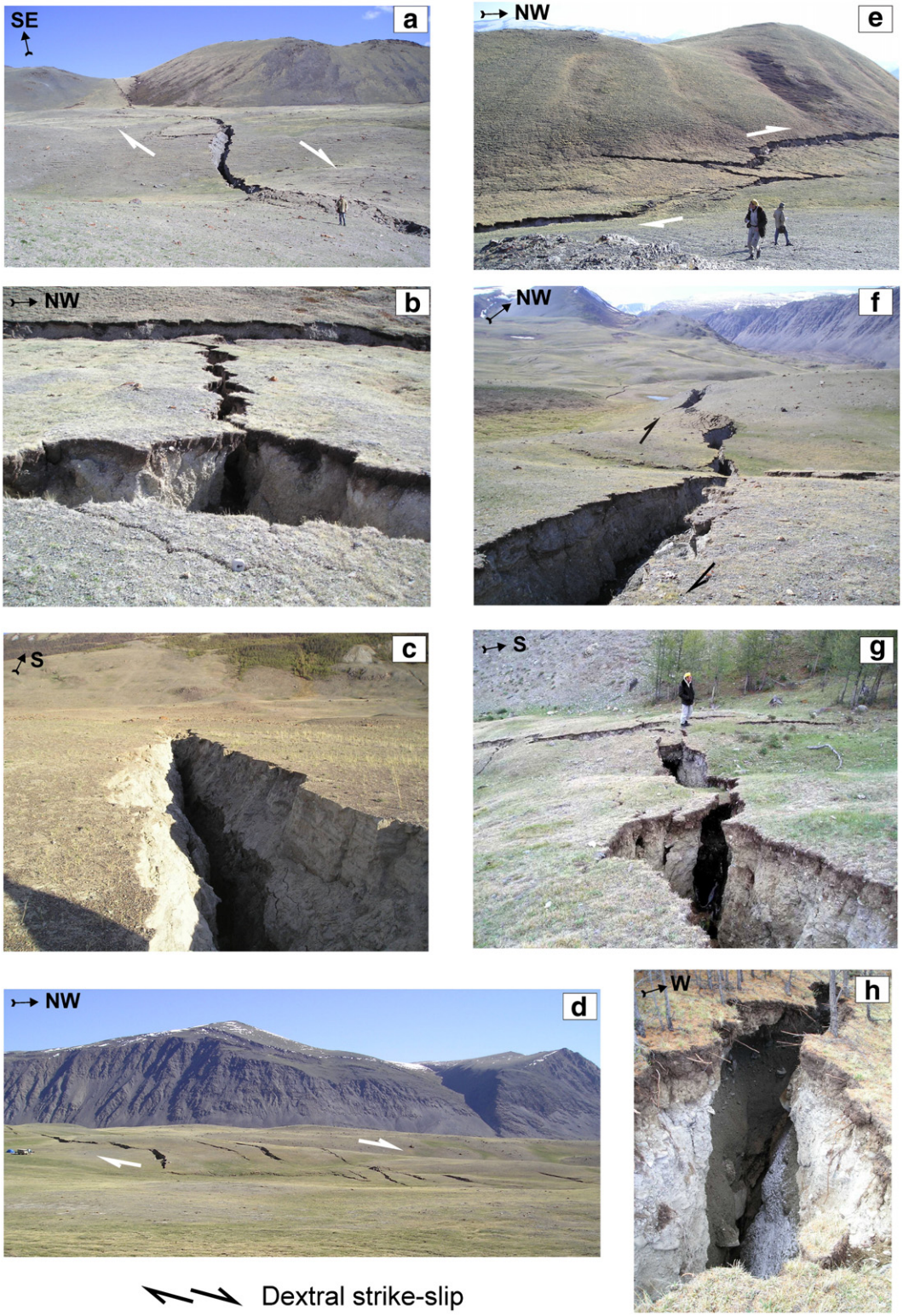

Fig. 4. Surface ruptures in the Pleistocene–Holocene sediments: (a) general view of the large rupture along the watershed of the Taltura and Kuskunnur Rivers; (b) site 0402, transverse fracture linking two sub-parallel ruptures (close up view of Fig. 4e); (c) site 0304, rupture in the Taltura River valley; (d) right-stepping en-echelon system of fractures; (e) site 0402, sub-parallel ruptures; (f) rupture between sites 0402 and 0401; (g) site 0202, junction between two ruptures; (h) site 0202, rupture at the interior part of the landslide.

compression that results from the convergence of the Hindustan and Eurasian plates, still persisting today, is the main driving force of the latest tectonic evolution of the region.

The Altai ranges and basins resulted from uplifted and relatively subsided neotectonic blocks (Fig. 1b). The seismic events of September–October 2003 occurred in the Southeastern Altai at the boundary between the North and South Chuya ranges and the Kurai-Chuya basin system (Fig. 1c). The main shock of the Chuya earthquake took place between the North Chuya range and Chagan-Uzun block. The latter separates the Kurai-Chuya basin system into two depressions. They are superimposed on the Riphean and Devonian metamorphic rocks and filled with Cenozoic sediments. The faults of the Kurai and Chuya basins and their mountainous frame are investigated mainly by palaeoseismological and geomorphological methods (Rogozhin et al., 1998; Rogozhin and Platonova, 2002; Novikov, 2004). The NW–SE faults are the major ones predetermining the present-day block structure of the area (Fig. 1b and c). The E–W fault separating the North and South Chuya neotectonic blocks is also a prominent one (Fig. 1c), running along the Taltura River valley. The NE–SW faults are secondary ones. According to most researchers (Rogozhin and Platonova, 2002; Novikov, 2004 and others), the E–W and NW–SE fault zones are the major seismogenic structures, though the variably-trending faults are also associated with features of the Pleistocene–Holocene reactivation. Palaeoseismic ruptures that are typical of earthquakes with M = 7.5 and greater are found within the Kurai-Chuya basin system and adjacent area (Rogozhin et al., 1998; Rogozhin and Platonova, 2002).

3. Methodology

In order to study the geometry of the fault zone and associated stress fields in the epicentral area of the Chuya earthquake, structural and tectonophysical observations were performed in several sites along the 30 km long segment between the Yelangash River and the Kuskunnur River (Fig. 2). This is an area of intensively dissected topography in the western part of the Chuya basin where the rupture system is clearly defined at the surface, crossing the valleys and watersheds of the rivers. Late Cenozoic sediments overlap the river valley and some of the watersheds. Bedrock is mainly found in the sides of the water stream and mountainous tops.

The data have been collected and processed by the approaches applied in tectonophysics for studying fractures of various scales. The description, photography and measurements of spatial (azimuths of dip and/or direction, angle of dip) and kinematic (slickensides and displacement of markers) parameters of the fractures and other associated structures (folds, push-ups) in unconsolidated sediments and in bedrock were made in 36 sites during our field investigations (Fig. 2). We paid a special attention to the study of zones of crushing, fracture cleavage and fracturing in general as well as relationships between the fractures produced by the Chuya earthquake and previous ones. Detailed mapping of the newly-formed rupture system within some segments of the axial part of the zone was made with 12 channel Garmin handheld GPS navigators (GPS 12 × L model).

Most of the measurements of shear fractures has been performed in 21 of 36 sites. These measurements have been used for i) the construction of diagrams, ii) the identification of conjugate shear fracture systems and iii) the reconstruction of the stress field (Fig. 3a and b). The well-known concept of relations between tectonic fractures and orientations of the principal stresses (Gzovsky, 1975; Hancock, 1991; Twiss and Moores, 1992) is a base for the analysis. To reveal the conjugate fracture systems, the diagrams were analyzed following the statistical method of Nikolaev (1992). The fundamentals of the method have been recently described in detail by Lunina et al. (2005b)

Fig. 5. Site 0401b, extensional fracture associated with strike–slip movement.

and therefore we remind only the main conditions that should be fulfilled to separate the conjugate shear fracture systems from other fracture sets (Fig. 3a and b): (1) the maxima on the fracturing diagram must possess the prominent opposite scattering derived from the tectonic stress field; (2) the maxima must lie on a great circle of projection; 3) the angle between the conjugate maxima must be not less than 30°. Following the identification of shear fracture systems, the principal stress axes can be inferred based on: the line of intersection of the conjugate faults is the intermediate stress axis (σ_2); the compressional stress axis (σ_1) bisects the acute angle between the fault planes; and the tensional stress axis (σ_3) bisects the obtuse angle (Anderson, 1951; Gzovsky, 1975; Hancock, 1991; Twiss and Moores, 1992).

At site 0301, the measurements of slickensides allowed to apply multiple inverse method (Yamaji, 2000, the software is available at http://www.kueps.kyoto-u.ac.jp/~yamaji/PDS/indexe.html) for reconstruction of the stress field.

As a whole, the obtained individual solutions revealed the local variations of state of stress in the seismogenic fault zone. To determine the initial regional stress field that stimulated the Chuya earthquake and caused the formation of the whole deformational pattern, we integrated all the data (geometry of the seismogenetic features, measured displacements, analysis of the fracturing diagrams and slickensides).

4. Results

4.1. Co-seismic deformations in the unconsolidated sediments

The co-seismic deformations in the unconsolidated sediments consisting of Pleistocene–Holocene boulder-pebbly,

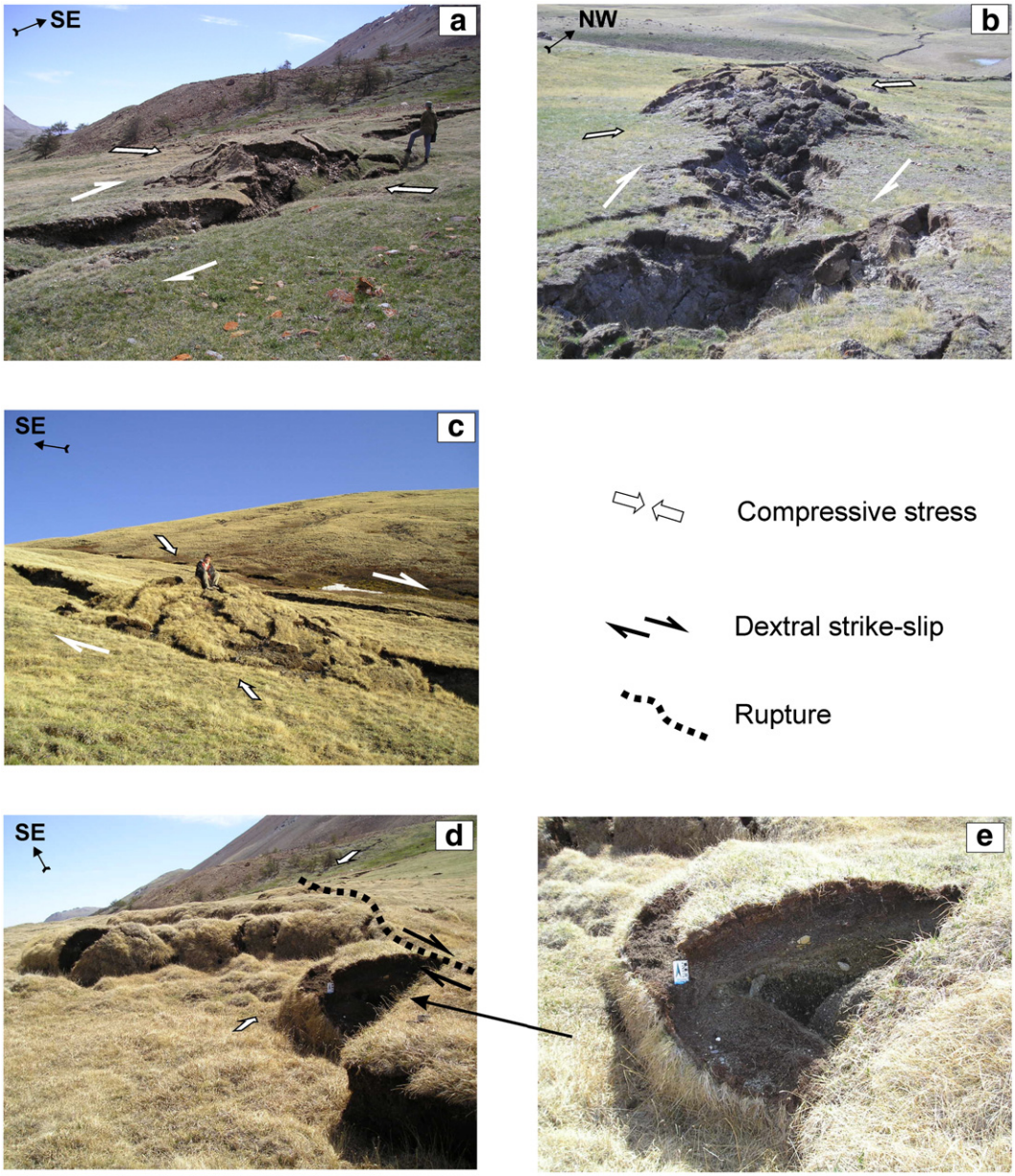

Fig. 6. Contractional structures: (a, b, c) Push-ups observed at site 0601 (a), between sites 0401a and 0401b (b) and between sites 0401b and 0402 (c); (d, e) folds at site 0601.

clastic, loamy and sandy deposits were intense. They are represented by the systems of strike–slip ruptures interpreted as *R*- and *R′*-shears (Fig. 4), extension fractures (Fig. 5) and contraction structures (Fig. 6). It is important to note that the longer ruptures which appeared on the surface and traced at a depth for several meters (as far as we could observe) were referred to primary ones. These ruptures were mainly used for further analysis. However, we also documented some secondary cracks that were only few meters long and shallow if those were of interest for kinematic interpretation.

The orientation analysis of the surface ruptures (Fig. 7a) shows the predominance of the NW–SE trending ruptures (280–350°) with maximum between 290° and 330° likely corresponding to *R*-shears. *R′*-shears are not so clearly defined and trend 350–30°. The strike–slip ruptures are characterized by opening from few centimeters up to some meters that is for the most part due to gravity. Fig. 7b and c document that the NW–SE and WNW–ESE fractures are dextral and the NE–SW and NNE–SSW are sinistral. The maximum displacement observed along the co-seismic rupture with a dextral strike–slip (trending 290°) is 2.5 m (site 0402). The maximum displacement of sinistral surficial ruptures is 0.2 m along fractures trending 10° and 25° (sites 0601 and 0603). Vertical displacements are less common: the largest normal offsets (1 m at site 0402) are typical of the NW–SE trending fractures, while the largest reverse offsets are typical of the ENE–WSW trending fractures. Large continuous ruptures of several tens to few hundreds of meters long are visible down to some meters in depth until clastic material fills them up. Eyewitnesses reported that a year after the Chyua earthquake speleologists could go into the ruptures up to a depth of 50 m.

The arrangement of strike–slip ruptures is clearly differentiated. In some cases, they are represented by one or two well-defined nearly parallel ruptures and smaller fractures (Fig. 4e and f). In places, individual transverse ruptures (Fig. 4b) complicate the pattern. The above-mentioned parts alternate with areas wherein the fractures show a right-stepping en-echelon geometry (Fig. 4d). The clearly defined fractures are mainly observed along slopes and ridge lines, while areas of diffuse deformation — in the lowered places with thicker unconsolidated sedimentary units. Within the junction areas between large *R*- and *R′*-shears (Fig. 4g), the geometry of the fault zone seems to be especially complicated and displacements along nearly parallel fractures can be of opposite character. A landslide of size ~1×0.85 km (Fig. 8) occurred within one of the junctions between large ruptures on the slope of the right side of the Taltura River valley. Two large old landslides are located alongside it. They are evidence of past catastrophic earthquakes in the Southeastern Altai.

The detailed study of the surface ruptures in the unconsolidated sediments gives the opportunity to visualize the dynamics and conditions of their growth. First, the ruptures commonly consist of small segments less than 1 m long that form conjugate fracture system (Fig. 9a). Locally, the mutually opposite displacements along these fractures produce rhombic blocks (Fig. 9b) and pull-apart (Fig. 9c). This determines a general S-shape of the fractures of various lengths and possibly reflects the character of the seismic wave propagation (variations of directions and amplitudes of seismic waves) in the elastic medium. Second, there is some evidence that the medium reacts to the dynamic impact as a homogeneous body during the process of fracture development in spite of the presence of numerous clastic inclusions of firm rocks and stumps (Fig. 9d, e and f).

The extension fractures are represented by 2–7-m wide ditches. They are usually located at the tips of the *R*-shears

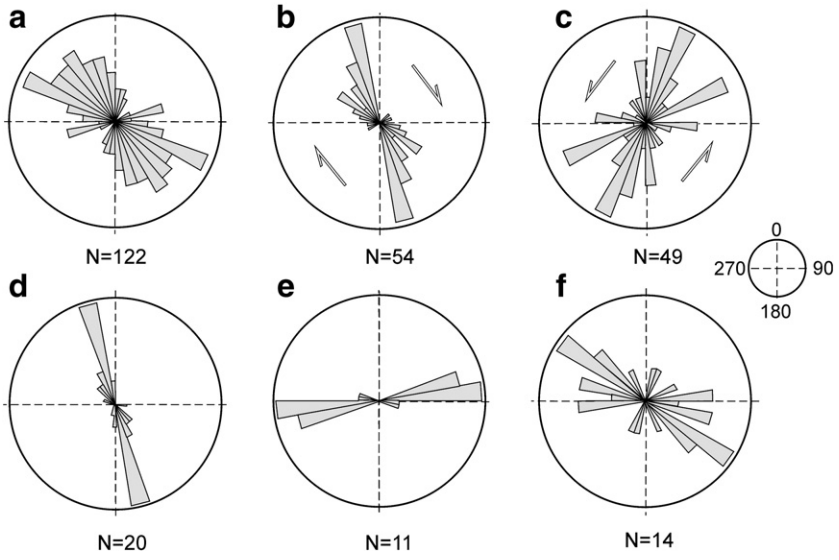

Fig. 7. Rose diagrams of directions of various structural elements within the broader fault zone: (a) co-seismic ruptures in unconsolidated sediments; (b) co-seismic fractures with dextral kinematics; (c) co-seismic fractures with sinistral kinematics; (d) extension fractures; (e) push-up axes; (f) large co-seismic ruptures dissecting the bedrock. N — number of measurements. Sector size is 10°.

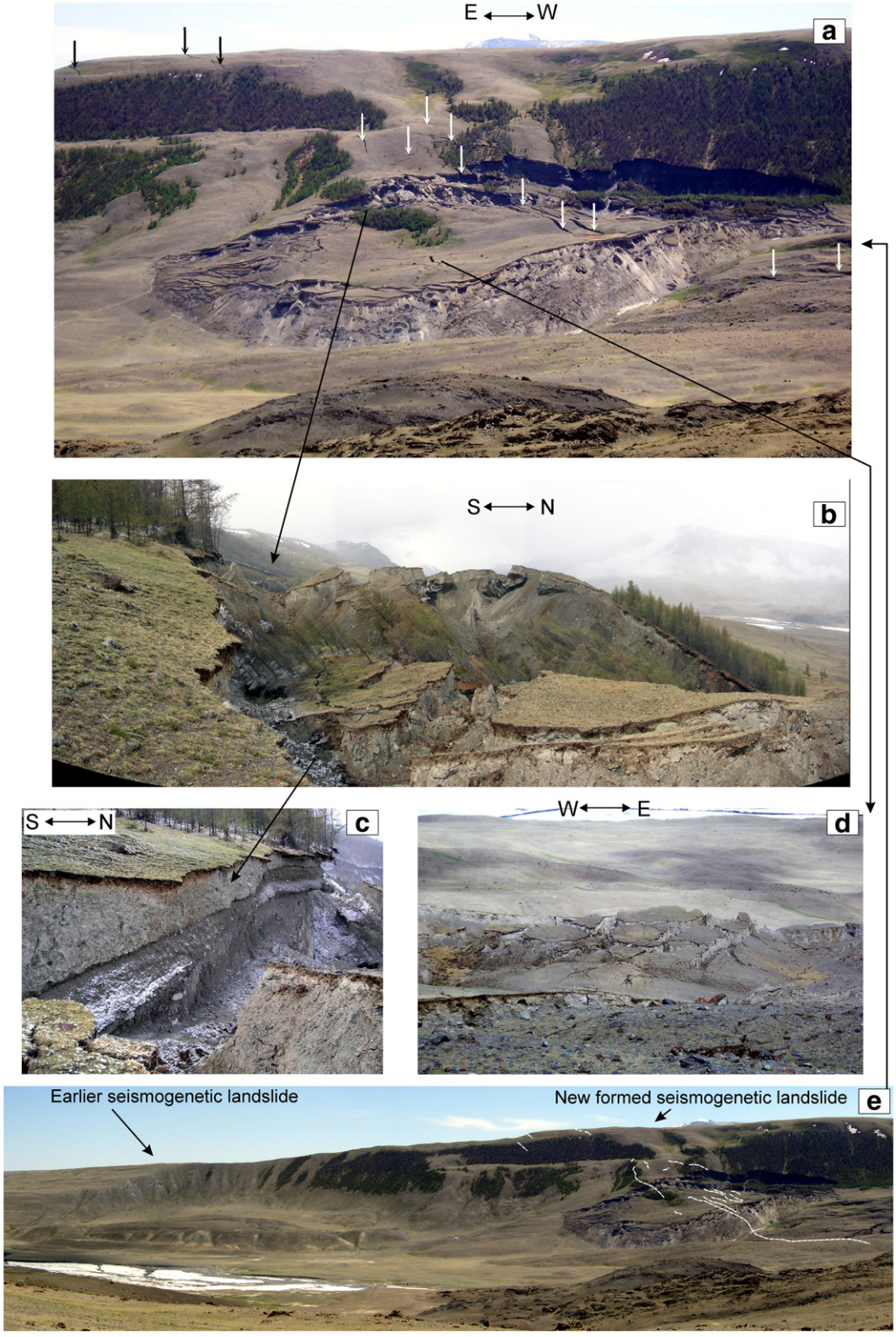

Fig. 8. Landslides in the Taltura River valley: (a) landslide produced by the Chuya earthquake, arrows show the major NW–SE ruptures; (b) interior part of the newly-formed landslide; (c) wall of loss of contact in the interior part of the newly-formed landslide; (d) fracture systems forming blocks in the landslide body; (e) previous and newly-formed seismogenetic landslides (according to Caputo, 2005a).

(Fig. 5). The contractional structures are expressed mainly by 10–15 m long push-ups (Fig. 6a, b and c). At site 0601, folds have been observed together with the push-ups (Fig. 6d and e). The extension fractures and the long axes of the push-ups are oriented perpendicular to each other, trending 340–350° and 70–90°, respectively (Fig. 7d and e).

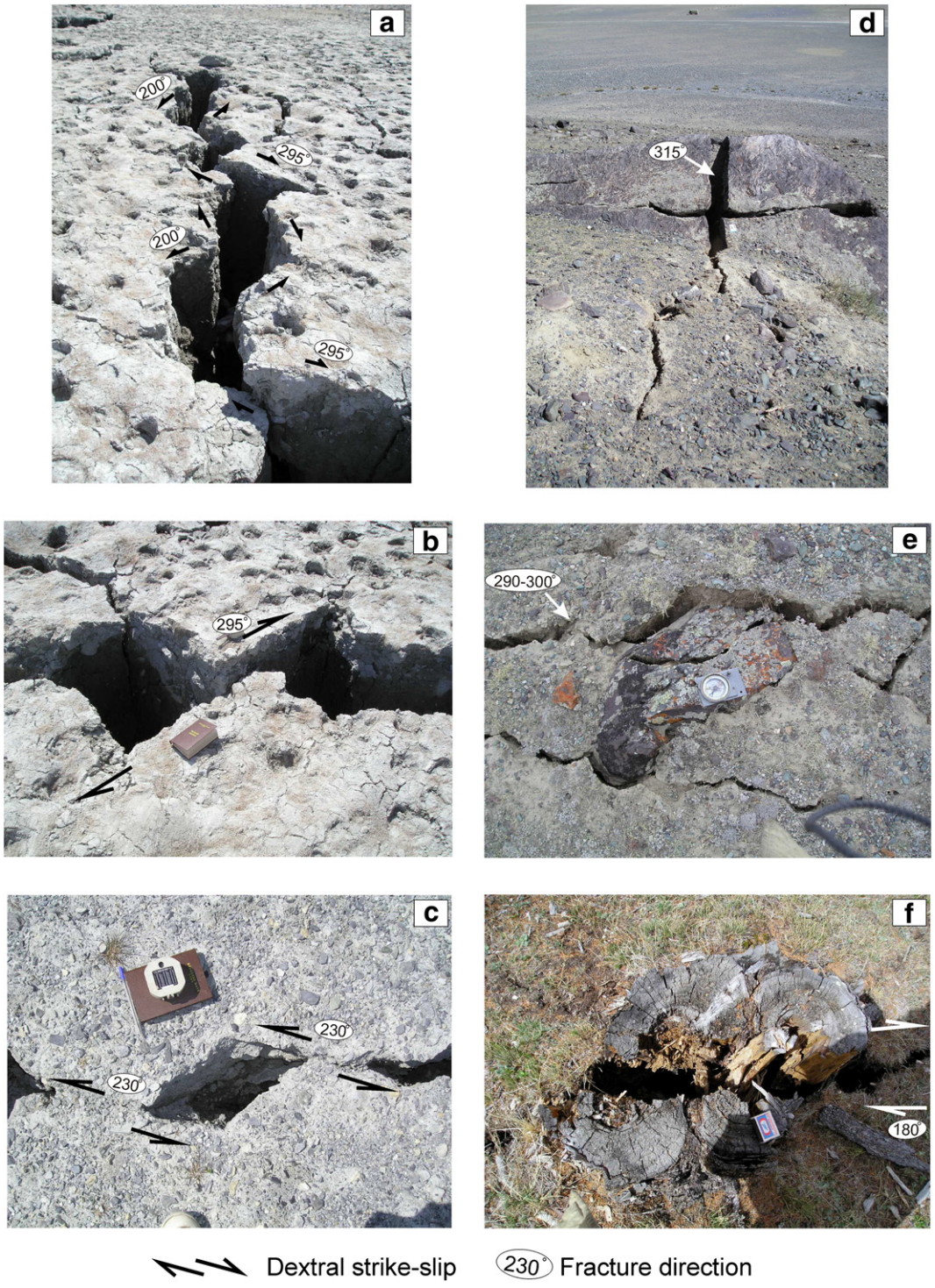

Fig. 9. Examples of surface ruptures in unconsolidated sediments; (a) site 0401, rupture consisting of variably oriented segments; (b) site 0401, rhombic blocks; (c) site 0401, pull-aparts; (d) site 0602, rupture splitting the boulder more than 3 m in dimension; (e) site 0601, fractures cutting pebble and soil in the same direction; (f) site 0202, dextral strike–slip offset of the stump along the N–S rupture near the junction of several ruptures.

The analysis of the data on the co-seismic deformations in the unconsolidated sediments shows that the pattern of the surface ruptures produced by the Chuya earthquake is associated with a NW–SE trending dextral shear zone (Fig. 10).

4.2. Co-seismic deformations in the bedrock

In the bedrock, mainly Devonian crystalline schists, the co-seismic deformations of the Chuya earthquake are observed at 9 sites (0203, 0204a, 0205, 0301, 0301a, 0501, 0502a, 0503, and

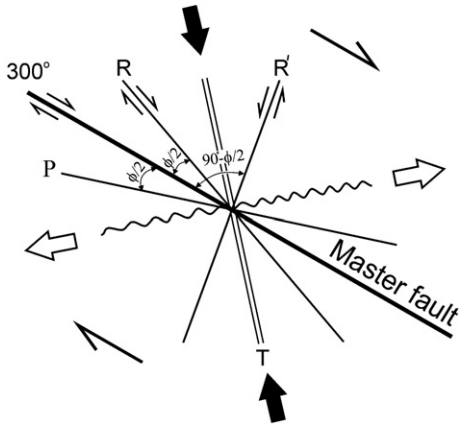

Fig. 10. Riedel model of the right simple shear adapted to structural situation in the fault zone of the Chuya earthquake. Double parallel line represents the orientation of extension (T) fractures; wavy line represents the axial orientation of the push-up. *P* — *P* fractures; *R*- and *R′* are synthetic and antithetic shears respectively; ϕ — angle of internal friction. Black arrows are shortening axes; white arrows are lengthening axes (modified from Sylvester, 1988).

0504, Fig. 2). These are manifest in the reactivation (opening) of existing zones of schistosity or individual fractures with displacements up to few tens of centimeters (Figs. 11, 12a and b) and in the formation of new ruptures and zones of coarse crushing (Figs. 12c, d, e and 13).

The preexisting fault zones trending NW–SE and E–W proved to be the most favorable for the reactivation. Strongly crushed zones resulted in a large volume of rock involved in the deformation. This occurred as small offsets along fractures up to 2 m in length. A clear example of such development of co-seismic deformations was observed at site 0301, in the fault zone traced along the Taltura River with a visible width of fracturing zone not less than 80–100 m, azimuth of dip 355–0° and dip angles of 80–85°. Co-seismic ruptures 0.1–0.3 m in opening formed in the less-fractured bedrock along the healed zone of schistosity (Fig. 11a and c). They could be traced continuously in the crystalline rocks and unconsolidated sediments. Both reactivated and newly-formed fractures have a right-stepping en-echelon geometry relative to large ruptures (Fig. 11b).

Obvious traces of rapid growth of the existing high-angle fractures have been observed at site 0504 (Fig. 12a and b) in the right side of the Kuskunnur Valley. Moreover, it is remarkable that the zones of the coarse crushing (0.2–3.0 m in width) formed during the Chuya earthquake in the low-fracturing, almost monolithic, crystalline schists with cohesive sub-horizontal schistosity and scarce sub-vertical fractures (Fig. 12c, d and e). The distinct surface ruptures of tens to few hundreds of meters in length were mapped on the NW slope and top of the Nomodokl Mount at sites 0502a and 0503 (Fig. 13). The ruptures with various trends formed the complex junction, within which both dextral and sinistral strike–slip offsets occurred along individual segments forming a large rupture zone trending NW–SE. The same situation is typical of the ruptures trending NE–SW. The opposite offsets along the fractures of the same trend are local and due to various rate of movement and rotation of blocks that formed in the fault junction.

The predominant direction of the mapped co-seismic ruptures cutting the bedrock is 300–320° (Fig. 7f). There are

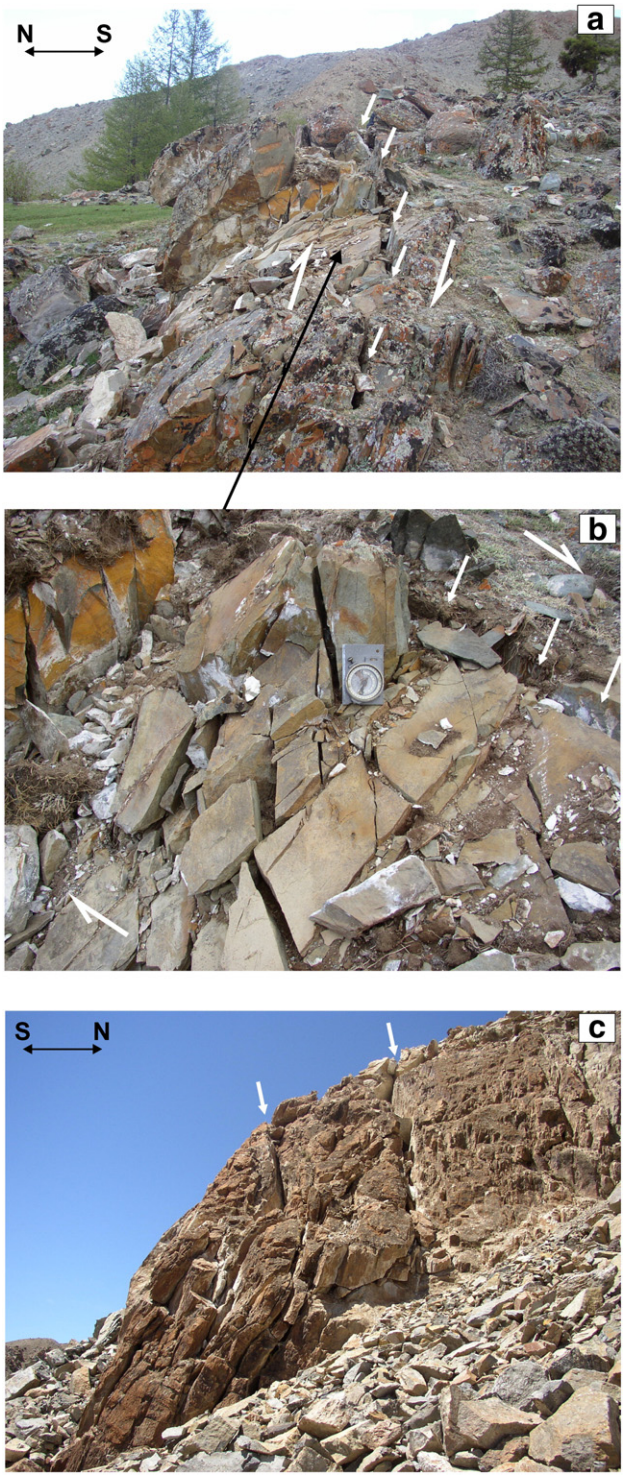

Fig. 11. Seismogenetic reactivation (opening) of the existing fault zones at the bedrock: (a) site 0205, reactivation of the NW–SE trending fault with dip angle 85–88°; (b) newly-formed and reactivated fractures representing a right-stepping en-echelon secondary fracture system with respect to the larger rupture; (c) 0301a, opening of large fractures in a wide fault zone.

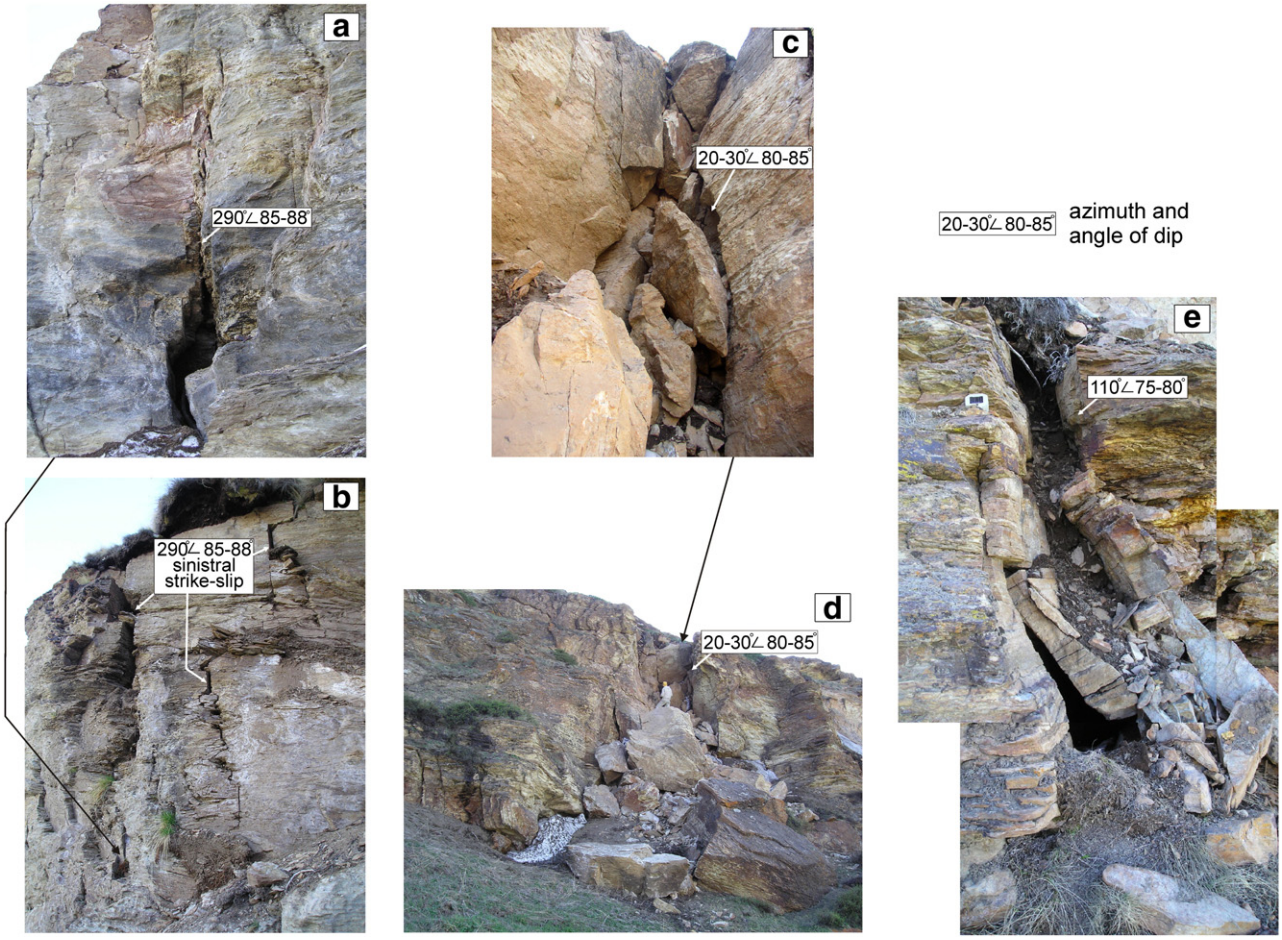

Fig. 12. Site 0504, co-seismic deformations in the bedrock at the right side of the Kuskunnur River valley: (a, b) reactivation of pre-existing high-angle fractures; (c, d, e) zones of coarse crushing associated with the Chuya earthquake.

also reactivated faults trending 330–340°, 20–30° and 80–110°. In synthesis, the direction of the co-seismic ruptures in bedrock, their kinematics, structural features, and fracture relationships are similar to those observed in unconsolidated sediments.

4.3. Newly-formed and preexisting fault patterns

Using the data on the co-seismic deformations in the unconsolidated sediments and bedrock, we have compiled maps showing the geometry and the kinematics of the NW–SE trending rupture zone produced by the Chuya earthquake (Figs. 14 and 15). The co-seismic fault pattern is characterized by all structural features that have been previously described. First of all, this is an uneven arrangement of the surface ruptures. In some sector, the rupture consists of an individual major fault (Fig. 15d), while locally a system of smaller faults arraying as en-echelon (Fig. 15c). The combination of all types of the newly-formed structures as a whole represents the unified paragenesis. Along most part of the fault zone, the NW–SE and NNW–SSE trending faults are mainly dextral strike–slip ones (locally with a normal component due to gravity). The NE–SW and NNE–SSW trending planes are sinistral strike–slip faults and the nearly E–W trending faults are reverse ones with an insignificant strike–slip component. In places, left-lateral movements occurred on NW–SE trending ruptures (Fig. 15c) and right-lateral movements — on the NNE–SSW and NE–SW ones (Fig. 15e). These latter structures are interpreted as second order features due to a locally and temporarily re-oriented stress field (Caputo, 2005b).

In order to estimate the extent to which the fault zone of the Chuya earthquake has inherited the preexisting faults, we analyzed zones of crushing, schistosity and fracturing recorded in the Pre-Cenozoic bedrock and compiled a map of the fault pattern that existed before the 2003 rupturing earthquake (Fig. 16). This pattern is mainly characterized by some major NW–SE and nearly E–W trending faults with crushing zones thicker than 5 m, and by secondary NNE–SSW trending faults with crushing zones of less than 5 m in thickness. The kinematic indicators within the crushing and fracturing zones of major NW–SE and nearly E–W trending faults show that both were strike–slip ones in the past. However, their spatial relationship does not indicate that these are conjugate faults. Most probably, the faults developed independently under different stress regimes and each of them could have generated significant seismic events. A simultaneous development of the NW–SE and NNE–SSW faults that are apparently conjugate strike–slip

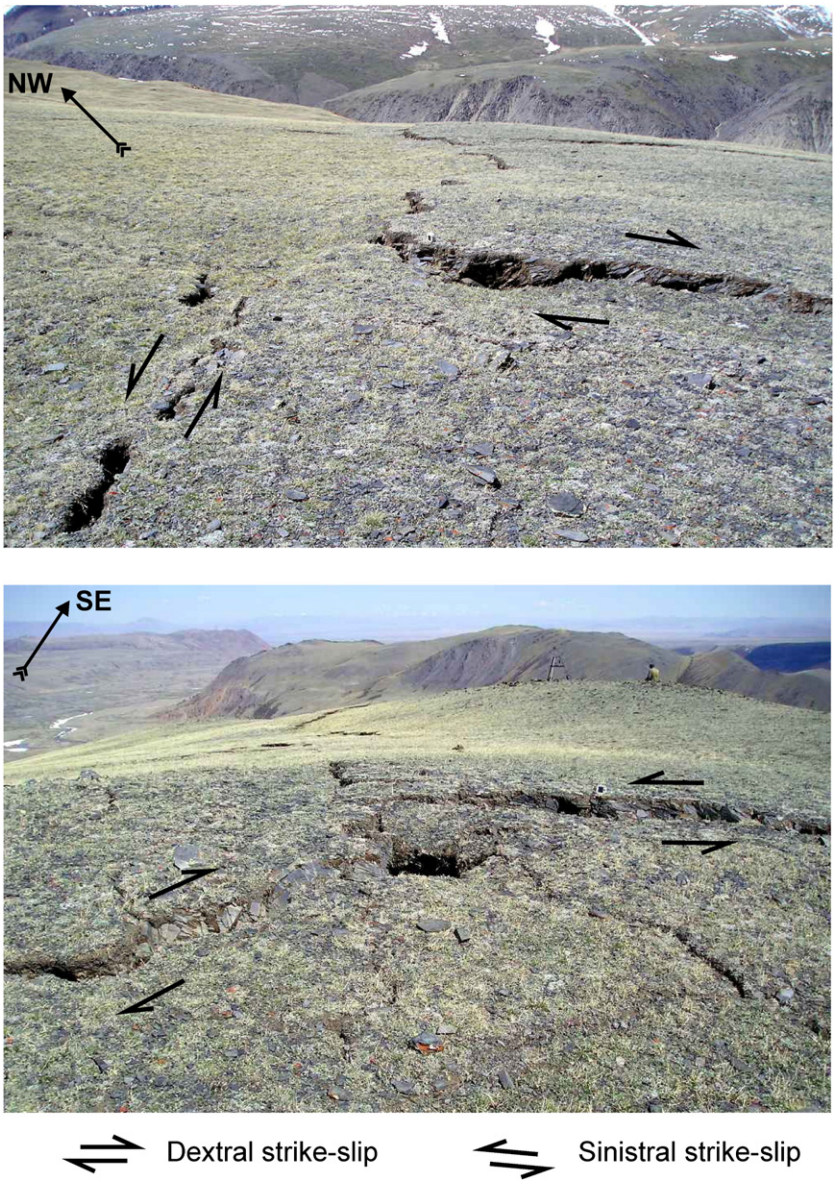

Fig. 13. Site 0503, junctions between ruptures produced during the Chuya earthquake in bedrock of the Nomodokl Mount.

ones occurred in the nearly N–S compression and nearly E–W tension that characterise the later stage of tectonic deformations.

The comparison between the existing faults and the newly-formed ones shows that the fault zone of the Chuya earthquake largely inherited the older structures (Fig. 16). For example, the long WNW–ESE and NW–SE co-seismic ruptures have opened along preexisting zones of schistosity (Fig. 11a). The smaller en-echelon fracture systems are often located at some angle to them. We suggest that the NW–SE trending faults mapped in the bedrock are the result of a crustal scale fault zone that started to develop in pre-Cenozoic, but some of its segments are active till the Pleistocene–Holocene. It is noteworthy that the southeastern segment of the co-seismic fault pattern changes the direction from NW–SE to nearly N–S, thus inheriting a possible fault running along one of the N–S valleys (Fig. 1c, right lower corner) that unfortunately has not clear surface and structural expression. Reactivation of the nearly E–W fault trace along the Taltura River during the Chuya earthquake is less pronounced. Large surface ruptures with similar direction reactivated and formed south and north of it.

4.4. Analysis of fracturing diagrams and stress fields

The diagrams of fracture measurements show that with rare exception, in unconsolidated sediments the most clearly defined are the systems corresponding to *R*- and *R′*-shears of the major NW–SE dextral strike–slip zone (Fig. 3a). The maxima of NW–SE, NNW–SSE and NE–SW, NNE–SSW fractures likely correspond to *R*- and *R′*-shears, respectively. In the bedrock, where the existing NW–SE fractures occur, *R*- and *R′*-shears are also well pronounced (sites 0203, 0205, 0206, 0302, 0501, 0503, 0504 in Fig. 3b). As this takes place, the structural pattern observed in the diagrams is often similar to that of the Quaternary unconsolidated sediments. However, in the

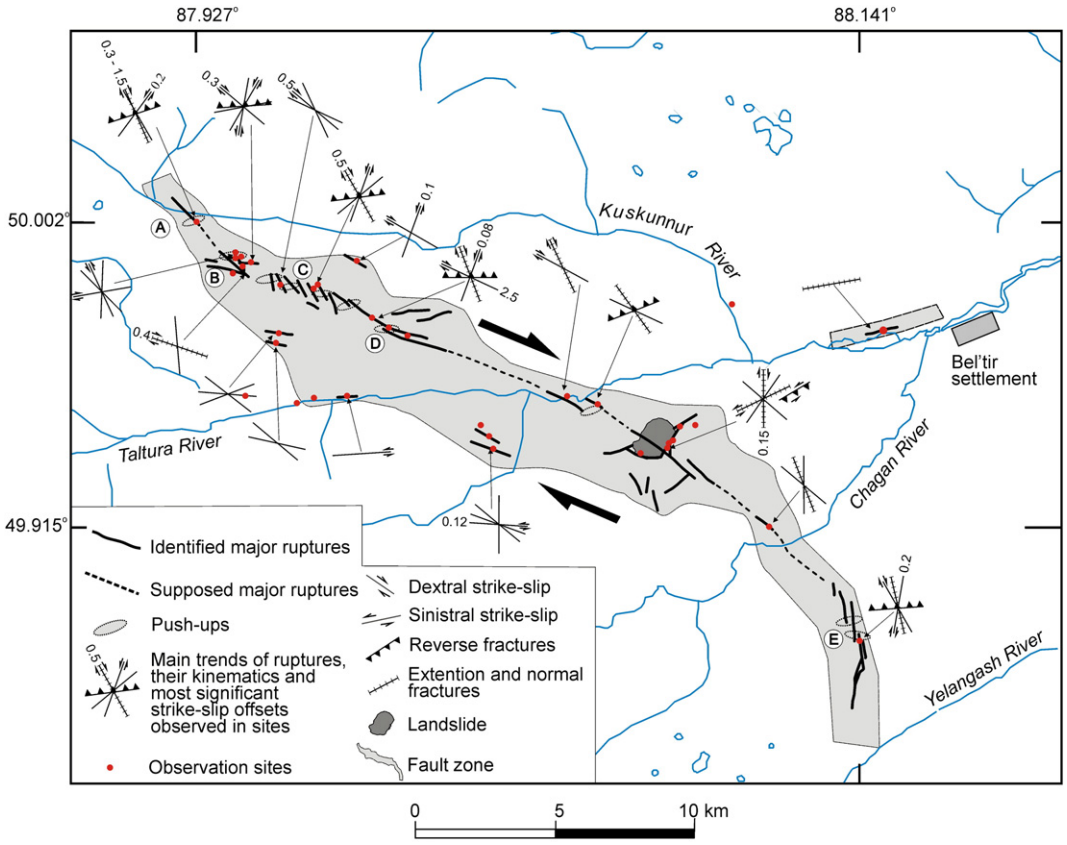

Fig. 14. Geometry of the primary surface ruptures produced during the Chuya earthquake. Capital letters in circle show locations of maps represented in Fig. 15a, b, c, d, and e, respectively.

preexisting nearly E–W trending fault zones, *R*-shears (sites 0402 and 0102 in Fig. 3b), *R′*-shears (sites 0502 and 0204 in Fig. 3b) or both of them (site 0301 in Fig. 3b) are often secondary structures as compared to the E–W fractures. Fig. 3a, b and c display that most of the *R*-shears and the major seismogenic fault dip towards NNE with a mean angle of 80°.

The fracturing diagrams analyzed with the Nikolaev's method (1992) show one set of conjugate shear fracture systems at most locations (Fig. 3a and b). Two conjugate sets occur more rarely and there is not conjugate system at site 0502 (Fig. 3b). The stress solutions inferred from conjugate fracture systems affecting unconsolidated sediments and bedrock are also very similar (Fig. 3a and b). Most of them correspond to a transcurrent regime (σ_1 plunges 0–30°, σ_2 — 61–90°, and σ_3 — 0–30°). The σ_1 principal axis trends NNW–SSE (locally nearly N–S) and σ_3 trends nearly E–W. At sites 0103, 0401 (Fig. 3a) and 0205 (Fig. 3b), σ_1 and σ_3 locally rotate (σ_1 nearly E–W and σ_3 nearly N–S). Similar changes can be explained by a short-term variations of the relative stress values during fracturing in a rock massif (Seminsky, 2003; Lunina and Gladkov, 2004; Caputo, 2005b). In this research, two stress solutions with opposite directions of σ_1 and σ_3 (sites 0401 in Fig. 3a and 0205 in Fig. 3b) have been obtained from the analysis of the fractures newly-formed and reactivated during one sequence of seismic events. This is an evidence that the principal stress axes can reorient almost instantaneously.

In specific cases, stress regime changes from one site to another or in the same site. This is only due to an increase of plunge angle of σ_1. For example, the solutions corresponding to transtension (when σ_1 is 31–60°, σ_2 is 31–60°, and σ_3 is 0–30°) have been obtained at sites 0503, 0302 and 0204 (Fig. 3b). The solution corresponding to pure tension (σ_1 plunges 61–90°, σ_2 — 0–30°, and σ_3 — 0–30°) was obtained in site 0301 (Fig. 3b). At the same time, the transcurrent regime with the unvarying nearly E–W direction of σ_3 has been reconstructed at site 0301 (Fig. 3d) following the multiple inverse method (Yamaji, 2000). Taking into account the location of this site in the zone of high-angle fault traced along the Talture River, we suppose that such variations of the stress field are affected by this structure. The distribution of the stress trajectories in the area affected by the Chuya earthquake is shown in Fig. 17. In the sector between Chagan and Yelangash rivers the principal stress axes rotate clockwise and so the compressional stress axis trends NE–SW. The strike of the co-seismic fault zone in this segment also changes from NW–SE to nearly N–S.

Temporal and local variations of the stress regime are also reflected in the focal mechanisms of the aftershocks. Most of the fault plane solutions are of strike–slip type, but there are also reverse and normal fault planes (Fig. 18). According to the seismological (Fig. 18) and structural data (Figs. 3 and 17), the orientation of the compressive stress often deviates from a general N–S to alternately NW–SE and NE–SW.

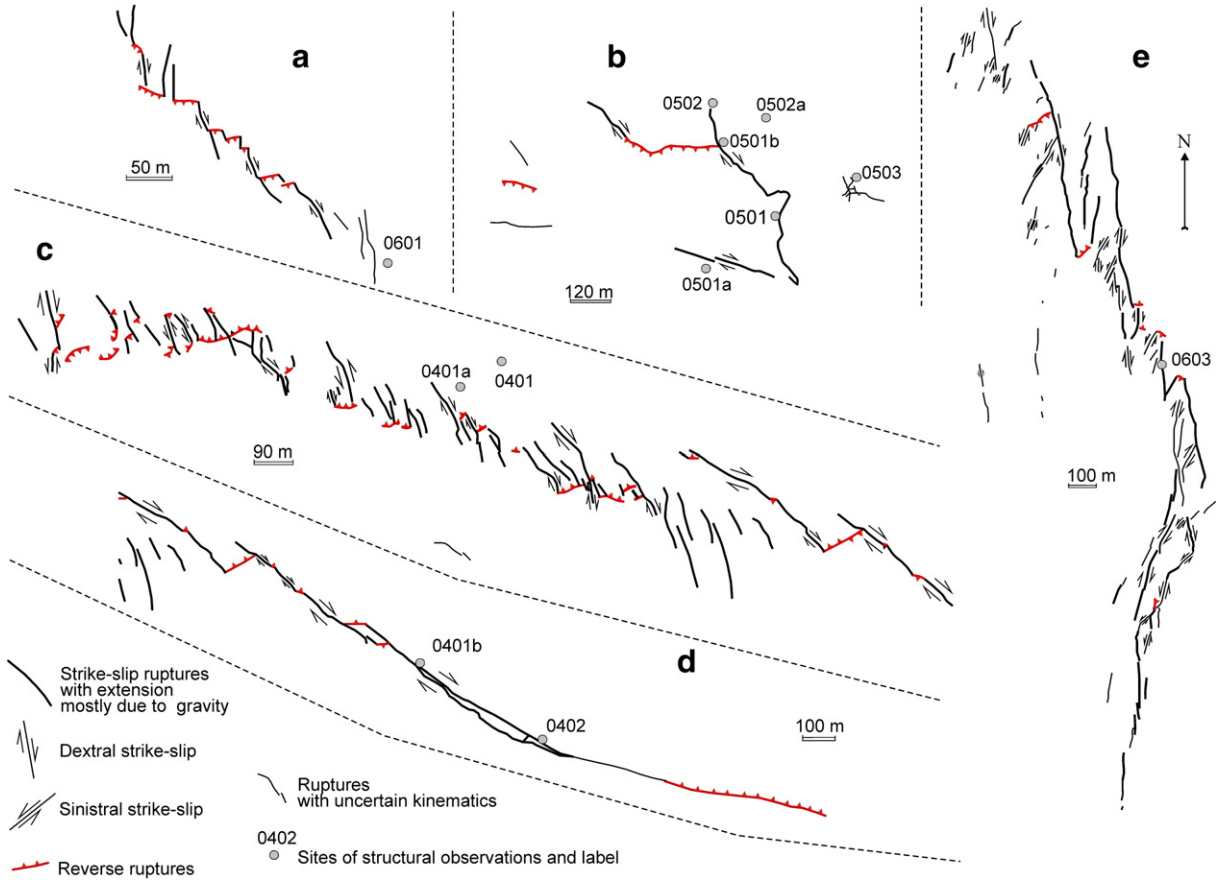

Fig. 15. Detailed view of the fault zone: (a–e) letters correspond to those in Fig. 14.

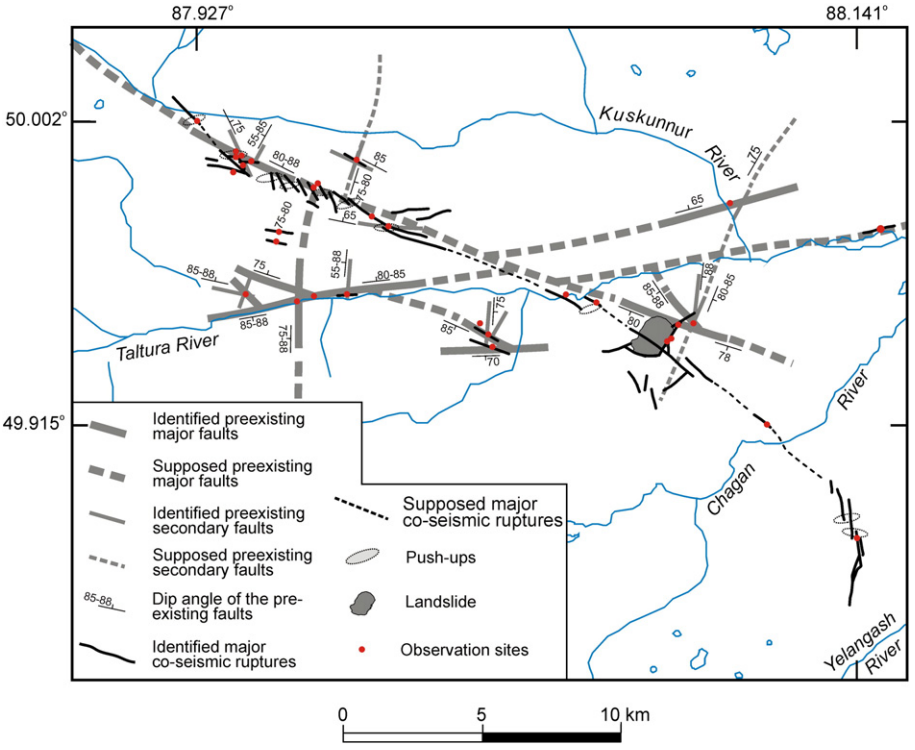

Fig. 16. The fault pattern that existed before the Chuya earthquake and superimposed co-seismic ruptures.

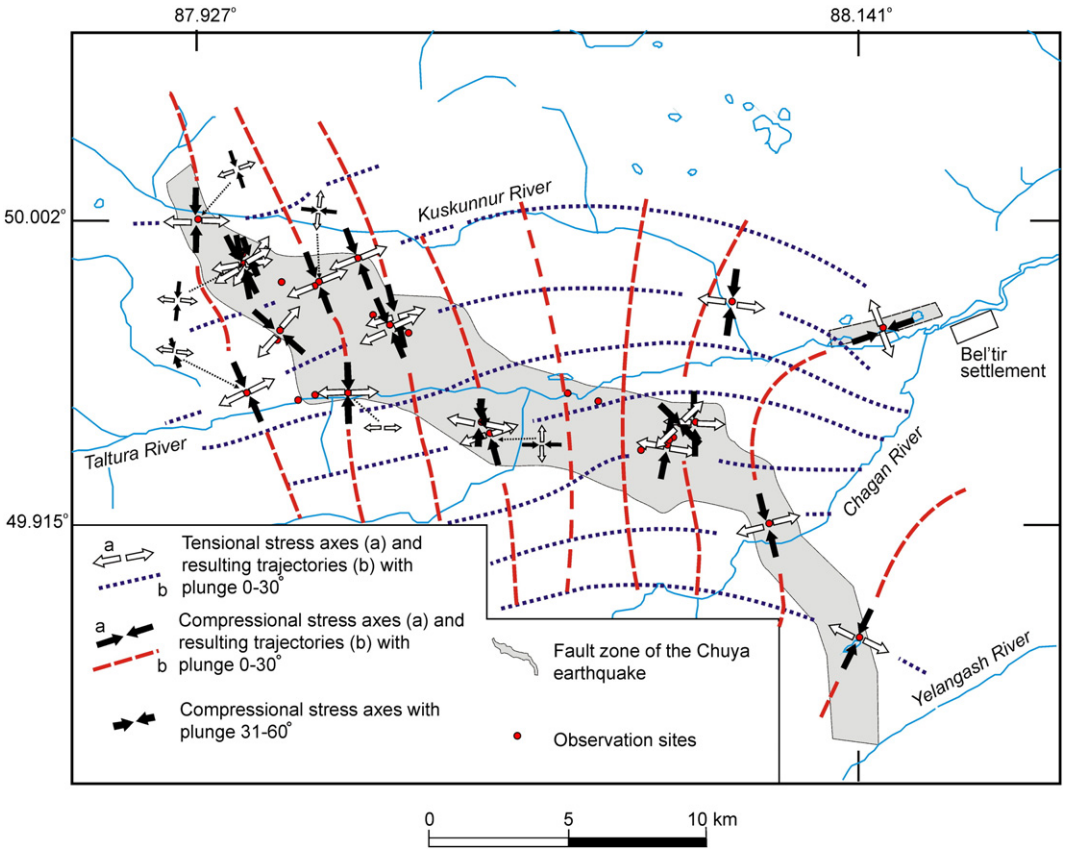

Fig. 17. Distribution of the stress trajectories in the investigated area.

In summary i) the fault geometry (directions of *R*- and *R*′-shears, extension fractures and contraction structures), ii) the measured offsets (Figs. 7 and 10), iii) the analysis of the fracture diagrams (Fig. 3a, b and c) and slickensides (Fig. 3d) suggest the occurrence of an initial transcurrent regime that produced the structural pattern of co-seismic deformations during the Chuya earthquake, is characterized by a NNW–SSE (almost N–S) compressive stress and a ENE–WSW (almost E–W) tensile stress. This interpretation is in agreement with the focal mechanism of the main shock of September 27, 2003, 11:33 (Fig. 18, see also Harvard SMT Catalog, http://www.seismology.harvard.edu).

5. Discussion

In Rock Mechanics, the term "fault zone" refers not only to the master fault itself but also to a greater rock volume where both brittle and ductile deformations are genetically connected with faulting. Accordingly, fault zones can be characterized by a complex and laterally variable structural fabric (Seminsky, 2003). Our results show that the pattern of the surface ruptures and other deformations associated with the Chuya earthquake exactly corresponds to a major fault zone trending NW–SE in the frame of a Riedel model (Fig. 10). The maximum width of the fault zone determined by location of extreme sites, where NW–SE co-seismic ruptures have been mapped, is 4–5 km (Fig. 14).

As has been shown by experiments (Wilcox et al., 1973; Harding and Lowell, 1979; Bornyakov and Adamovich, 2000; Seminsky, 2003) and confirmed by the analysis of natural structures (Pachell and Evans, 2002; Young et al., 2001; Seminsky, 2003; Escuder Viruete et al., 2003; and many others), long-term evolution of fault zones that are localized even in an homogeneous substratum under an uniform load along their strike and a constant deformation rate is non-uniform. We investigated the strike–slip fault zone that formed instantaneously at the geological time scale because it occurred within tens of seconds — few minutes, as a minimum, and 5 days, as a maximum, considering the main shock of September 27, 2003 (Ms=7.5) and the strongest aftershock of October 1, 2003 (Ms=7.1, Harvard SMT Catalog, http://www.seismology.harvard.edu). The complex fault zone is characterized by, first, a space variability of the fracture pattern and second, by the reorganization of the stress field surrounding individual fault segments wherein σ_1 and σ_3 are swapped or σ_1 deviates from the horizontal close to the newly-formed or already existing faults. This local variation of the initial dynamic setting occurred mainly in the vicinity of the nearly E–W faults impeding the release of accumulated compressive stresses in the N–S direction because of the high-angle fault planes. As a result, small strike–slip offsets of the simple shear type, sometimes with small openings, took place along the E–W trending high-angle faults. New nearly E–W surface ruptures

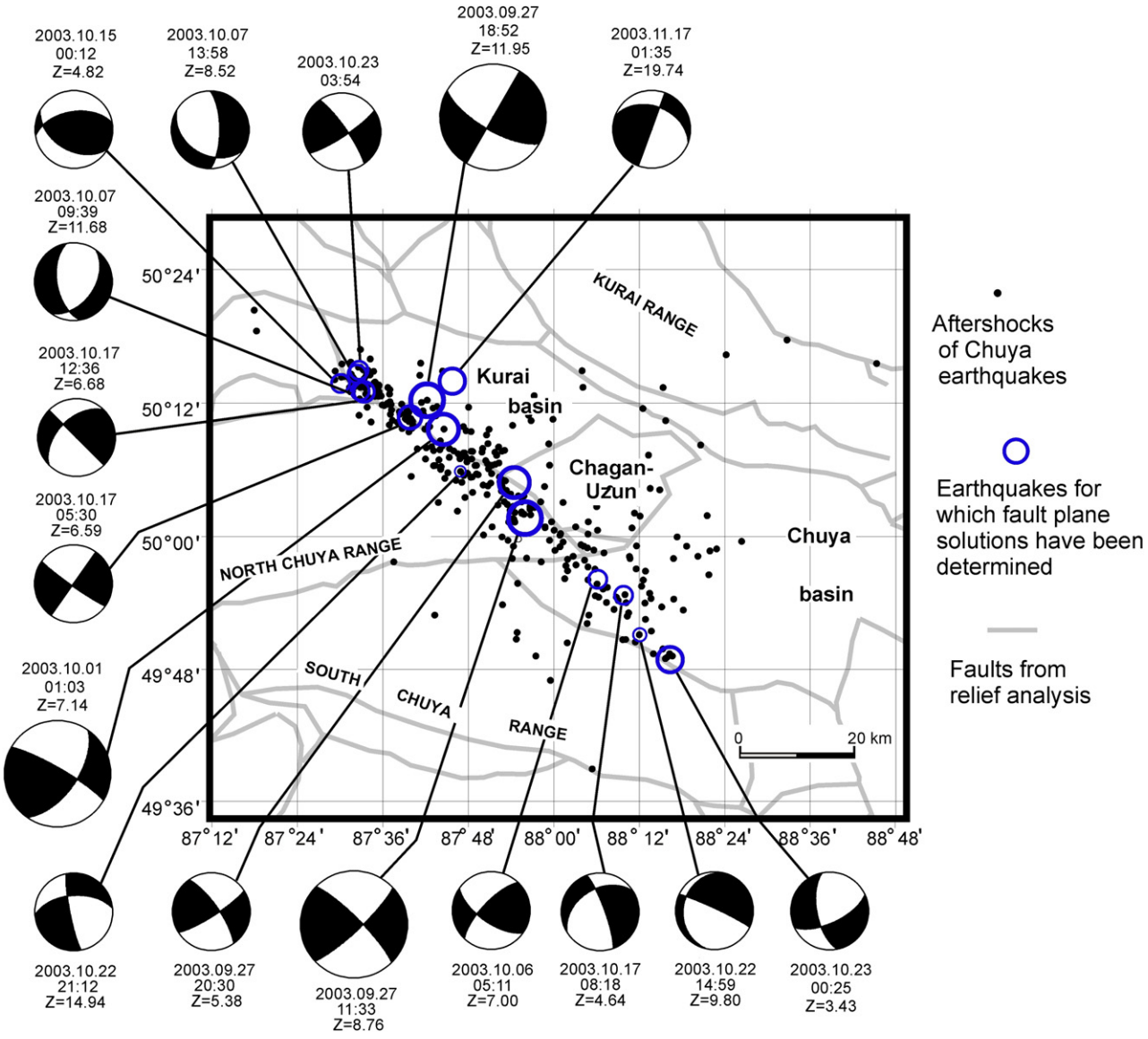

Fig. 18. Main shock and aftershocks focal mechanisms of the Chuya earthquake. The data on the location of the epicenters, focal depth (Z) and mechanisms have been obtained by Geophysical Survey of the Siberian Branch of RAS (after Emanov and Leskova, 2005).

with a reverse displacement formed aside from preexisting faults with the same trend (Fig. 14).

According to physical and structural criteria, the fracturing process associated with the creation of a major fault zone can be subdivided into several stages (Harding and Lowell, 1979; Kim et al., 2003; Seminsky, 2003). For example, Seminsky (2003) separates the early and late disjunctive stages and the stage of full breaking based on the moments of appearance of the principal structural reorganization and the occurrence of the master fault (Fig. 19). If the mapped pattern of co-seismic surface ruptures (Fig. 14) is compared with the theoretical model (Fig. 19), it is evident that the fault zone of the Chuya earthquake is in a late disjunctive stage (segment B–C in Fig. 19). The master fault has not yet formed at this stage but its segments are already clearly defined. According to Fig. 19, the stressed crustal volume, where the co-seismic ruptures formed, has passed through a short-time period of elastic state (segment O–A) and strengthening (segment A–B), thus entering the state of loss of substratum strength (segment B–C), getting through the moment of principal structural reorganization after the first fractures appeared. It is important to emphasize that this interpretation concerns only the newly-formed pattern of co-seismic deformations. We may just suppose that the preexisting fault that was inherited by the ruptures of the Chuya earthquake is in the same late disjunctive stage or in a stage of full breaking in a depth below 8.76 km (location of hypocenter). The case of a master fault developed completely at a depth and looks as a wide zone more close to the surface is illustrated in published papers (Fig. 22d in Sylvester, 1988; Figs. 2 and 13 in Philip and Meghraoui, 1983, Fig. 3 in Matrosov et al., 2004). Every new seismic event contributes in developing a larger fault zone. What observed in the investigated area suggests that the common laws of the deformation of solid bodies apply even close to the surface and with high rates of movements.

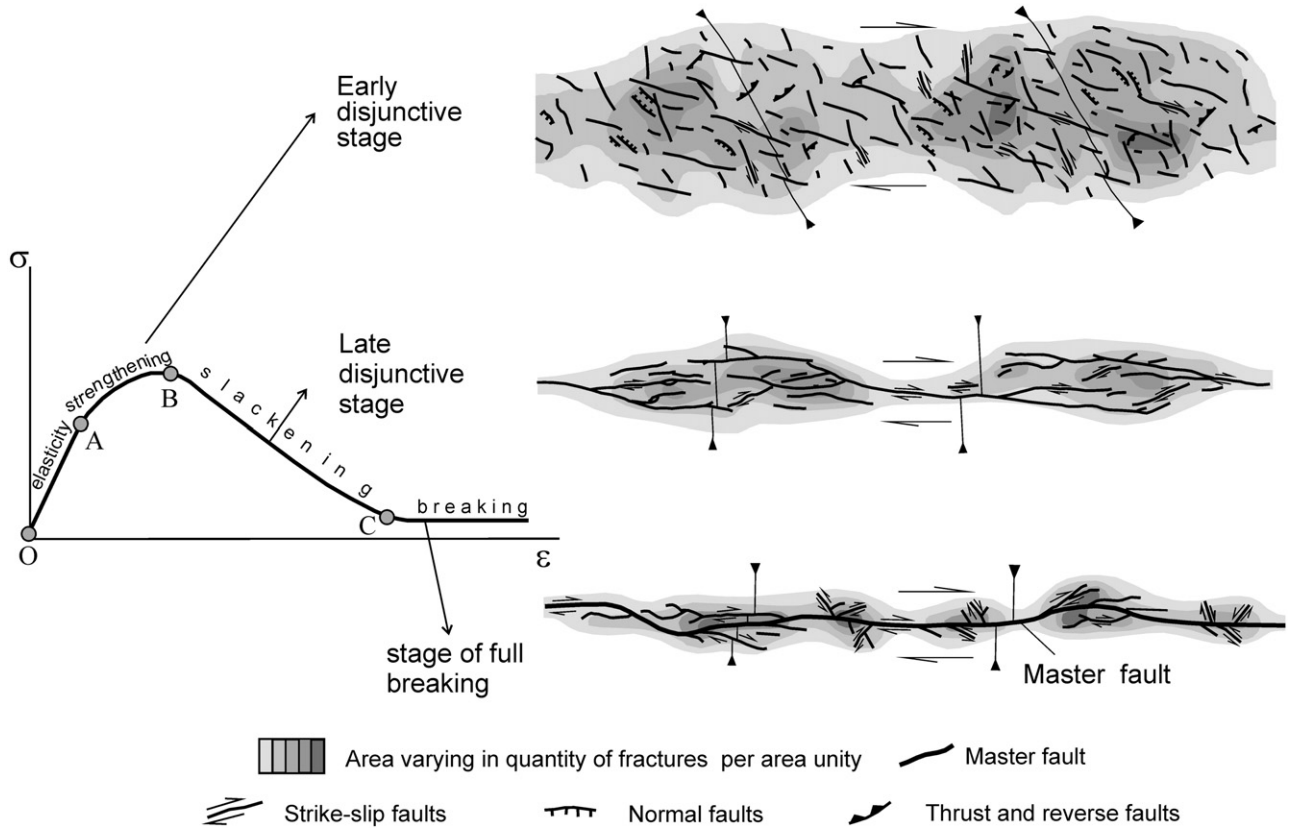

Fig. 19. Mechanical model for the formation of a fault zone through several seismic cycles. The principal stages of fracturing correspond to three characteristic segments on the curve "stress .σ) — strain (ε)" (after Seminsky, 2003).

The seismic event of September 27, 2003 is a demonstrative example of rupturing earthquake reflecting the present-day geodynamical regime in the Gorny Altai. The study of the pattern of co-seismic deformations at the surface of the earth crust and its comparison with a mechanical model of fracturing also suggests the applicability of this model to the analysis of near instantaneous deformations produced by strong earthquakes.

6. Conclusions

Our research allows characterizing in detail the pattern of co-seismic deformations of the Chuya earthquake on September 27, 2003 along a 30-km long segment and concluding the followings.

1. The co-seismic deformations of the earthquake affected both unconsolidated sediments as the *R*- and *R′*-shears, extension fractures and contraction structures, and bedrock with the reactivation of schistosity planes and individual fractures, development of new ruptures and coarse crushing zones.

2. The combination of all newly-formed structures is the paragenesis, where the NW–SE and NNW–SSE trending faults are dextral strike–slip faults (sometimes with a normal component, often due to gravity), the NE–SW and NNE–SSW trending faults are sinistral faults and the nearly E–W trending faults are mainly reverse faults with an insignificant strike–slip component. The same kinematics is observed along the preexisting reactivated fractures of the same directions, except for the nearly E–W trending faults, where the state of stress varied locally due to the occurrence of high-angle fault planes, that resulted in small strike–slip displacements.

3. The pattern of the co-seismic ruptures is consistent with a major NW–SE trending dextral fault zone with maximum width 4–5 km and associated with *R*- and *R′*-shears, extension fractures and contraction structures regularly oriented to each other. According to the mechanical model of Seminsky (2003), the observed distribution of fractures corresponds to the late disjunctive stage of faulting when the master fault has not completely formed yet but its segments have clearly defined.

4. The initial stress field that resulted in the whole structural ensemble of co-seismic deformations during the Chuya earthquake corresponds to a transcurrent regime with the NNW–SSE (almost N–S) oriented compressive stress and ENE–WSW (almost E–W) trending tensile stress. The state of stress in the newly-formed fault zone is relatively uniform. Local stress variations in the rock are expressed i) in minor deviations of σ_1 from N–S to NW–SE or to NE–SW, ii) in short-term variations of the relative stress values and iii) in increasing plunge angle of the σ_1 close to preexisting faults.

5. The development of co-seismic rupture pattern started in place wherein minor but stable changing of orientation of principal compressional stresses occurred: the σ_1 rotates slightly from N–S direction to east in the south-eastern part of fault zone and to west — in north-western part of fault zone.

6. If the mechanical model of fracturing is scaled at the crustal volume and compared with the geometry and kinematics of the dextral shear zone associated with the 2003 Chuya earthquake, it is possible to apply the same model to the analysis of near instantaneous deformations produced by strong earthquake. Therefore the fracturing process in widely different rocks follows the common laws of the deformations of solid bodies even close to the Earth surface and with high rates of movements.

Acknowledgements

The research has been partly supported by Siberian branch of Russian Academy of Science (Complex Integrated project SB RAS 2006 No 6.13), Russian Science Support Foundation and INTAS (grant No 05-109-4383). The first author considerable thanks Spyros B. Pavlides for the constructive discussion of the submitted results. We are grateful to Arkadi Karakhanyan and Vladimir G. Trifonov for thorough reviews, criticisms and advices that were very useful. Special thanks to Riccardo Caputo who contributed greatly to improvement of the manuscript.

References

Anderson, E.M., 1951. The dynamics of faulting. Edinburg. 206 pp.

Baljinnyam, I., Bayasgalan, A., Borisov, B.A., Cisternas, A., Dem'yanovich, M.G., Ganbataar, L., Kochetkov, V.M., Kurushin, R.A., Molnar, P., Philip, H., Vashchilov, Yu.Ya., 1993. Ruptures of major earthquakes and active deformation in Mongolia and its surrounding. Memoir Geological Society of America 181 62 pp.

Bornyakov, S.A., Adamovich, A.N., 2000. Mechanism of fault segmentation and character of segment interaction (from results of physical and mathematical simulation). Journal of Earthquake Prediction Research 8, 471–485.

Caputo, R., 2005a. Ground effects of large morphogenic earthquakes. Journal of Geodynamics 40, 113–118.

Caputo, R., 2005b. Stress variability and brittle tectonic structures. Earth-Science Reviews 70, 103–127.

Cunningham, W.D., Windley, B.F., Dorjnamjaa, D., Badamgarov, J., Saandar, M., 1996. Late Cenozoic transpression in southwestern Mongolia and the Gobi Altai-Tien Shan connection. Earth and Planetary Science Letter 140, 67–81.

Cunningham, W.D., Windley, B.F., Owen, L.A., Barry, T., Dorjnamjaa, D., Badamgarav, J., 1997. Geometry and style of partitioned deformation within a late Cenozoic transpressional zone in the eastern Gobi Altai Mountains, Mongolia. Tectonophysics 277 (4), 285–306.

Emanov, A.A., Leskova, E.V., 2005. Structure of the aftershock process of the Chuya (Gorny Altai) earthquake. Geology and Geophysics 46 (10), 1065–1072 (in Russian).

Escuder Viruete, J., Carbonell, R., Marti, D., Jurado, M.J., Perez-Estaun, A., 2003. Architecture of fault zones determined from outcrop, cores, 3-D seismic tomography and geostatistical modeling: example from the Albala granitic pluton, SW Iberian Variscan Massif. Tectonophysics 361, 97–120.

Geodakov, A.R., Ovsuchenko, A.N., Platonova, S.G., Rogozhin, E.A., 2003. Materials of preliminary study of the strong earthquake in 2003 in the Gorny Altay. Electronic Scientific Journal of Vestnik Otdelenia Earth Nauk 1 (21) URL: http://www.scgis.ru/russian/cp1251/h_dgggms/1-2003/screp-8.pdf. (in Russian).

Gol'din, V.S., Seleznev, V.S., Emanov, A.F., Filina, A.G., Emanov, A.A., Novikov, I.S., Vysotskii, E.M., Fateev, A.V., Kolesnikov, Y.u.I., Podkorytova, V.G., Leskova, E.V., Yarygina, M.A., 2004. The Chuya earthquake and its aftershocks. Doklady Earth Sciences 395A (3), 394–396.Engineering Translations from Doklady Akademii Nauk 395 (4), 534–536.

Gzovsky, M.V., 1975. Fundamentals of Tectonophysics. Nedra, Moscow. 536 pp. (in Russian).

Hancock, P.L., 1991. Determining contemporary stress directions from neotectonic joint systems. In: Whitmarsh, R.B., Bott, M.H.P., Fairhead, J.D., Kusnir, N.J. (Eds.), Tectonic Stress in the Lithosphere. Phil Transactions Royal Society London A, vol. 337, pp. 29–40.

Harding, T.P., Lowell, J.D., 1979. Structural styles, their plate-tectonic habitats, and hydrocarbon traps in petroleum provinces. American Assotiation of Petroleum Geologists Bulletin 63, 1016–1058.

Kim, Y.S., Peacock, D.C.P., Sanderson, D.J., 2003. Mesoscale strike–slip faults and damage zones at Marsalforn, Gozo Island, Malta. Journal of Structural Geology 25, 793–812.

Leontyev, A.N., Rogozhin, E.A., 1995. Long-term geological factors of seismicity (exemplified by the Sayan-Altai fold area). Journal of Earthquake Prediction Research 4 (3), 320–339.

Lunina, O.V., Gladkov, A.S., 2004. Fault pattern and stress field in the western Tunka rift. Russian Geology and Geophysics 45 (10), 1188–1199.Engineering Translations from Geology and Geophysics 45 (10), 1235–1247.

Lunina, O.V., Gladkov, A.S., Novikov, I.S., Agatova, A.R., 2005a. Tectonophysical analysis of fracture deformation zone of the Chuya Earthquake (September 27, 2003). Doklady Earth Sciences 401 (2), 197–199. Engineering Translations from Doklady Akademii Nauk 401 (1), 58–61.

Lunina, O.V., Gladkov, A.S., Novikov, I.S., Agatova, A.R., Visotsky, E.M., Emanov, A.A., 2006. Seismotectonic Deformations and Stress Fields in the Fault Zone of the 2003 Chuya Earthquake, Ms = 7.5. Gorny Altai Geotectonics 40 (3), 208–224.Engineering Translations from Geotektonika vol. No 3, 52–69.

Lunina, O.V., Mart, Y., Gladkov, A.S., 2005b. Fracturing patterns, stress fields and earthquakes in the Southern Dead Sea Rift. Journal of Geodynamics 40, 216–234.

Matrosov, V.A., Bornyakov, S.A., Gladkov, A.C., 2004. New approach to optimization of prediction of diamond-contained kimberlites. Doklady Akademii Nauk 395 (2), 220–223.

Nikolaev, P.N., 1992. In: Nikolaev, N.I. (Ed.), Methodology of Tectonodynamical Analysis. Nedra, Moscow. 295 pp. (in Russian).

Novikov, I.S., 1992. Morphotectonics of the Altai. SB RAS. "Geo" Press, Novosibirsk. 313 pp. (in Russian).

Philip, H., Meghraoui, M., 1983. Structural analysis and interpretation of the surface deformations of the El Asnam Earthquake of October 10, 1980. Tectonics 2 (1), 17–49.

Pachell, M.A., Evans, J.P., 2002. Growth, linkage, and termination processes of a 10-km-long strike–slip fault in jointed granite: the Gemini fault zone, Sierra Nevada, California. Journal of Structural Geology 24, 1903–1924.

Rogozhin, E.A., Bogachkin, B.M., Nechaev, Y.u.V., Platonova, S.G., Chichagov, V.P., Chichagova, O.A., 1998. Paleoseismological investigations on the territory of Russian (Gorny) Altai. Journal of Earthquake Prediction Research 7 (4), 391–413.

Rogozhin, E.A., Platonova, S.G., 2002. Focal zones of strong earthquakes in the Gorny Altai in the Holocene. OIFZ Press, Moscow. 130 pp. (in Russian).

Sanderson, D.J., Marchini, W.R.D., 1984. Transpression. Journal of Structural Geology 6, 449–458.

Seminsky, K.Zh., 2003. The inner architecture of the continental fault zones. Tectonophysical aspect. SB RAS. "Geo" Press, Novosibirsk. 244 pp. (in Russian).

Sylvester, A.G., 1988. Strike–slip faults. Geological Society America Bulletin 100, 1666–1703.

Trifonov, V.G., Makarov, V.I., 1988. Neotectonics and recent geodynamics of the mobile belts. Nauka, Moscow, pp. 239–272.

Twiss, R.J., Moores, E.M., 1992. Structural geology. W.N. Freeman and Company, New York, p. 532 pp.

Vysotskii, E.M., Novikov, I.S., Agatova, A.R., Gibsher, A.S., 2004. Pleistoseist zone and tectonic position of the Chuya earthquake center in 2003. Doklady Earth Sciences 395A (3), 328–330Engineering Translations from Doklady Akademii Nauk 395 (4), 499–502.

Wilcox, R.E., Harding, T.P., Seely, D.R., 1973. Basic wrench tectonics. American Assotiation of Ptroleum Geologists Bulletin 57, 74–96.

Yamaji, A., 2000. The multiple inverse method: a new technique to separate stresses from heterogeneous fault-slip data. Journal of Structural Geology 22, 441–452.

Young, M.J., Gawthorpe, R.L., Hardy, S., 2001. Growth and linkage of a segmented normal fault zone; the Late Jurassic Murchison-Statfjord North Fault, northern North Sea. Journal of Structural Geology 23, 1933–1952.